2002-01-01

Flow Patterns in a Two-Roll Mill

Christopher Hills

Technological University Dublin, chris.hills@dit.ie

*Article Submitted to ***Journal title****

FLOW PATTERNS IN A TWO-ROLL MILL

by CHRISTOPHER P. HILLS

(Lincoln College, Oxford, England OX1 3DR)
e-mail: chris.hills@lincoln.ox.ac.uk *tel: +44 1865 288090*

Abstract

The two-dimensional flow of a Newtonian fluid in a rectangular box that contains two disjoint, independently-rotating, circular boundaries is studied. The flow field for this two-roll mill is determined numerically using a finite-difference scheme over a Cartesian grid with variable horizontal and vertical spacing to accommodate satisfactorily the circular boundaries. To make the streamfunction numerically determinate we insist that the pressure field is everywhere single-valued. The physical character, streamline topology and transitions of the flow are discussed for a range of geometries, rotation rates and Reynolds numbers in the underlying seven-parameter space. An account of a preliminary experimental study of a two-roll mill is also given. Photographs confirm the salient features predicted by our theoretical study.

1. Introduction

The Taylor-Couette problem, in which a fluid is contained between two independently rotating, co-axial, circular cylinders has been widely studied for over a century. Since an initial solution due to Stokes [1], a corroborating experimental treatment by Couette [2] and the landmark study by Taylor [3], this basic viscometer has been recognised as a paradigm for stability studies in fluid dynamics. A major ambition of such investigations has been to study and understand the mechanisms of flow transition in rotating systems, first to primary instabilities (characterised by Taylor cells) and subsequently to chaos and turbulence. Experiments have had a profound influence on the Taylor–Couette problem, not only in identifying the parameter bounds of various flow regimes, but also by suggesting the structure of theoretical solutions. It is perhaps not too surprising that considerable attention has been paid to generalisations of this basic viscometer that are also amenable to small scale experiments. For example, the classical Taylor–Couette arrangement has been extended by considering elliptic

containers ([4]), single cylinders in a rectangular or square domain ([5], [6], [7]) and eccentric circular cylinders ([8]). However, in all of these studies, the experimental convenience of the original Couette experiment is preserved largely at the expense of analytical simplicity. DiPrima [9], [10] have shown that an analytical solution can be obtained by asymptotic means when an eccentric, two-cylinder geometry involves a small intrinsic length scale as in, for example, a journal bearing.

In this paper we are interested in yet another generalisation, the two-roll mill, formed by inserting a second disjoint internal cylinder into the flow. The cross-sectional domain is, therefore, triply-connected. The pair of internal cylinders have the potential to produce strongly straining flows which, on physical grounds, we must expect to influence the stability properties of the system. The intrinsic complexity of a finitely bounded two-roll mill system inevitably means that a theoretical investigation will require a numerical treatment. However, the unbounded triply-connected cross-section has been discussed analytically although it is clear from these studies that careful attention must be paid to the nature of the far-field flow. Jeffery [11] found that it was impossible to find a simple Fourier series solution in bi-polar coordinates for which the flow vanished at infinity. In particular, he showed that for his method, with two equal cylinders rotating at the same speed in opposite senses, the far-field flow has to be a uniform stream but, somewhat disconcertingly, there is then no resultant force on the cylinders! Watson [12] resolved this paradox by modifying a Fourier-series for the Stokes equations to include a pair of line vortices at the cylinders' centres. When the inner solution is matched to an appropriately decaying solution of the full Navier-Stokes equations in the far-field limit, it was found that the resultant force on the cylinders was properly non-vanishing. Watson [13] extended his work to allow for a uniform stream past two rotating cylinders and found that this produces a lift force on the cylinders of the same order as the drag. Carlotti [14] have numerically plotted the streamlines for the Watson Fourier series, determining the coefficients by using a least squares criterion.

Experimental studies of the finitely bounded two-roll mill configuration have almost exclusively focused on instabilities. Three years after the original work of Taylor [3], Tarada [15] observed the formation of "a periodic pile of collar-shaped vortices" around two rotating cylinders. More recently Carlotti [14] and Vladimirov [16], both employing a square bounding domain, confirmed the Tarada vortices as the primary instability. For their specific geometry Vladimirov [16] gave a quantitative measurement of the critical Reynolds number for this transition ($Re_{\text{crit}} \sim 209$). Carlotti [14] classified subsequent transitions at higher Reynolds numbers. However, since both of these last two studies are only presently available in report form we include in §5 a preliminary report of two-roll experiments using the same apparatus as Carlotti [14]. For the case of a circular outer boundary, Price [17] experimentally studied the character of the two-dimensional base flow but his principal concern was with the bifurcations of the three-dimensional flow. Mullin [18] later extended this work showing that,

the two-cylinder configuration need not exhibit low-dimensional chaos but rather can resemble the features of totally disordered motion.

As regards theoretical studies of the two-roll mill, Price [17] obtained the Stokes solution appropriate to his experimental set-up using numerical techniques. Later Price [19] investigated in some detail the flow transitions of the Stokes flow generated in a two-roll mill confined in a circular boundary using a least squares approach and a series expansion in the complex plane. More recently, Koh [20] numerically analysed a particular two-roll mill contained in a square box but their study is flawed by an incorrect assumption regarding flow symmetry (see §2.2). Non-Newtonian behaviours produced in a two-roll mill are clearly a separate issue. They have been studied by Harrison [21] and Singh [22].

In this paper we determine the steady, two-dimensional flow of a Newtonian viscous fluid due to a two-roll mill in a rectangular domain (see Figure 1). The numerical solutions we find represent the primary flow before the onset of any instability and will act as the basis for subsequent stability studies. The mill problem is characterised by a seven-parameter space, $\mathcal{D}$ [see (2.6)], five of whose parameters specify the geometry. Our numerical code is flexible enough to investigate any point within $\mathcal{D}$ and, in particular, we analyse the influence of geometry, rotation ratios and Reynolds number on the streamline patterns of the mill. To resolve the flow pattern we employ a standard finite-difference scheme with an adaptive grid routine that reconciles a Cartesian grid (dictated by the rectangular confining boundary) with the circular internal boundaries. In Section 2, we set down the governing equations and give a brief discussion of our choice of grid, the implementation of the finite-difference method and the checks applied to our solution.

It is clearly impractical to tackle exhaustively the entire five-dimensional parameter space that defines the geometry and we illustrate salient features of the two-roll mill by two representative geometries [see (2.7)]. In the first, $\mathcal{G}_1$, the bounding box is square and two equal cylinders are symmetrically placed on the horizontal mid-line of the box. The cylinders diameters are one quarter of the box height. The second configuration, $\mathcal{G}_2$, relates to a more elongated box (side ratio $2 : 3.5$) with the cylinders again symmetrically placed on the mid-line but this time their diameters are one half the box height. The experiments of both Vladimirov [16] and Carlotti [14] use a square container, the former directly corresponding to $\mathcal{G}_1$ and the latter having slightly smaller cylinders.

In §3 we concentrate on co- and counter-rotation for configurations $\mathcal{G}_1$ and $\mathcal{G}_2$ and a range of Reynolds numbers when the angular speeds are equal. We find that for co-rotation the characteristic feature is a saddle point within the streamline pattern, lying midway between the cylinders. Figures 4-6 illustrate that this feature is preserved under increasing inertia. For both geometries there are three identifiable regions of the flow domain. In the neighbourhood of each cylinder the flow is trapped inside the figure-of-eight streamline and follows an almost circular path. Outside the separatrix the main flow encompasses both cylinders. The third domain relates to recirculation regions lying beyond streamlines of

separation that intersect the outer boundary. The nature of these regions is influenced by the intrinsic geometry. For the square geometry, $\mathcal{G}_1$, the recirculation regions occupy the full width of the box whereas in the rectangular geometry, $\mathcal{G}_2$, the recirculation regions take the form of corner eddies. The fluid circulates in opposite senses on either side of these separating streamlines. When the effects of inertia are included (see Figures 5, 6) the symmetries associated with Stokes flow are broken. In particular we observe a change in the shape of the recirculation regions and a skewing of the streamline and vorticity patterns that increases as the Reynolds number progressively grows. In the case of cylinders counter-rotating with equal angular speed the co-rotating saddle point is essentially replaced by a streamline of separation between the cylinders. The flow around each cylinder is similar in appearance to a single cylinder configuration. Eddies form at the four corners of the box (see Figure 7) and once again inertia causes the streamlines to skew. However, it is found that for counter-rotation the flow can only be pursued for Reynolds numbers that are a fraction of those for the co-rotating regime before a numerical instability manifests itself.

In §4 we consider the extent to which the topological characteristics of the flow (centres, saddle points and separation points) are influenced by rotation ratios in the range $\Omega \in (-1, 1)$. Equally important is the effect of varying Reynolds number and geometry. Specifically, for the configuration $\mathcal{G}_2$ we consider in detail a transition between the extremes of the co- and counter-rotation discussed in §3. The sequence of intermediate states relates to the symmetry-breaking cases when the cylinders rotate at different speeds. The topological features of these intermediate states will be constrained by the Euler characteristic [see (4.1)] that is fixed by the underlying flow topology and relates algebraically the number of saddle points, centres and separation points that any two-dimensional scalar field may possess over the domain. In other words, as we vary the rotation ratio Ω, the streamline features should always maintain a fixed Euler characteristic and Figures 8 and 9 show that our numerically determined intermediate states do indeed conform with this condition.

In §5 we briefly describe a sequence of experiments with a two-roll mill contained in a square box closely allied to the geometry $\mathcal{G}_1$. By using glycerine, suitably diluted with water, a range of Reynolds numbers [$Re \in (0, \sim 200)$] is possible for modest rotation rates of the cylinders. The series of photographs in Figure 11, for various Reynolds numbers and rotation ratios, shows a satisfying qualitative agreement with our numerical predictions.

2. Problem description and solution scheme

2.1. The governing equations

We consider an incompressible (Newtonian) fluid of kinematic viscosity ν' confined in a rectangular domain of width d' and height $2L'$ which contains two distinct, circular cylinders of radii r'_1 and r'_2. The two cylinders have centres lying on the horizontal axis of symmetry at distances a'_1 and a'_2 ($> a'_1 + r'_1 + r'_2$) from the

left-hand vertical boundary and rotate with angular speeds Ω_1', Ω_2' respectively (see Figure 1). The fluid motion is referred to a set of Cartesian axes centred halfway up the left-hand side of the rectangular bounding box. We assume a steady, two-dimensional flow with velocity and pressure fields, $\mathbf{u}'(x', y'), p'(x', y')$ respectively. It is convenient to work in terms of non-dimensional variables. As a typical length scale we take L' and as a typical velocity we use the speed of the left-hand cylinder. In addition, we set

$$\Omega = \Omega_2'/\Omega_1', \qquad p = L'p'/\nu'\Omega_1'r_1', \qquad Re = \Omega_1'r_1'L'/\nu', \tag{2.1a-c}$$

where Re is the Reynolds number. Both the experiments of Vladimirov [16] and those described in §5 indicate that as Re increases the initially two-dimensional flow will become susceptible to three-dimensional instabilities and eventually Taylor cells will form (see Figure 12). In this paper we are concentrating on the initial flow regime and will confine our attention to a range of Reynolds numbers low enough for the two-dimensional motion to persist.

In terms of the non-dimensional variables, the flow domain is bounded by the outer rectangle $\mathcal{B}$ ($x = 0,\, d$; $y = \pm 1$) and the inner circles $\mathcal{C}_\lambda$ with centres $(a_\lambda, 0)$ and radii r_λ, ($\lambda = 1, 2$). Then the usual no-slip condition on the boundaries require

$$\mathbf{u} = \mathbf{0} \text{ on } \mathcal{B}, \qquad \mathbf{u} = \Omega_\lambda'(-y, x - a_\lambda)/\Omega_1'r_1 \text{ on } \mathcal{C}_\lambda \quad (\lambda = 1, 2). \tag{2.2}$$

Since the motion of the incompressible fluid is two-dimensional we may write the velocity, $\mathbf{u}$, in terms of a Cartesian streamfunction $\psi(x, y)$ and then the only non-zero ($z-$)component of vorticity is given by $\omega = \nabla^2\psi$. The motion of the fluid is therefore governed by the system

$$\omega = \nabla^2\psi, \qquad Re\frac{\partial(\omega, \psi)}{\partial(x, y)} = \nabla^2\omega, \tag{2.3a}$$

$$\boldsymbol{\nabla}\psi = \mathbf{0} \text{ on } \mathcal{B}, \qquad \boldsymbol{\nabla}\psi = \Omega_\lambda' r_\lambda \widehat{\mathbf{n}}_\lambda/\Omega_1'r_1, \text{ on } \mathcal{C}_\lambda \quad (\lambda = 1, 2), \tag{2.3b}$$

where $\widehat{\mathbf{n}}_1$, $\widehat{\mathbf{n}}_2$ denote unit normal vectors to the cylinders.

While the problem (2.3a,b) is well-defined, condition (2.3b) is not particularly convenient for numerical work. From (2.2) we see that ψ is constant on $\mathcal{B}, \mathcal{C}_1, \mathcal{C}_2$ so that, without loss of generality, we may alternatively formulate the boundary conditions as

$$\psi = 0 \text{ on } \mathcal{B} \qquad \text{and} \qquad \psi = c_\lambda \text{ on } \mathcal{C}_\lambda, \quad (\lambda = 1, 2). \tag{2.4}$$

The constants c_λ are not known *a priori* and their values will emerge as part of our numerical scheme. To this end, we need a supplementary condition that will enable us to determine (via a root search) the c_λ. Two possible physical conditions suggest themselves as candidates: *i*) the circulation around each cylinder should be a known constant and *ii*) the pressure field, p, should be single-valued

throughout the flow field. By numerical experimentation it was found that the pressure boundary condition expressed as the contour integral

$$\oint \boldsymbol{\nabla} p . \mathbf{dr} = 0 \tag{2.5}$$

was far superior to the circulation criterion in pinpointing the values of the c_λ and it is the condition we adopt. It has been used previously by Lewis [5] in his treatment of the single cylinder rotating within a square container. Similar requirements of single-valuedness were imposed by DiPrima [10] in their study of the flow produced in a journal bearing formed by two eccentric cylinders. In our problem, we found that the pressure integral was almost linearly related to the inputted c_λ's which enabled accurate values for which (2.5) vanished to be quickly determined to within a specified precision. The contour chosen was typically a rectangle between two and four grid points from the boundary $\mathcal{B}$, well removed from any saddle points, separation contours or cylinder boundaries. When symmetry could be employed to relate the two constants c_1 and c_2 the contour encompassed both cylinders but for symmetry breaking cases and when checking the numerical integrity of the solution a contour was taken around each cylinder individually.

2.2. Symmetries of the triply-connected geometry

The triply-connected Taylor–Couette geometry, illustrated in Figure 1, lies in the seven-dimensional parameter space

$$\mathcal{D} = \big(r_1,\, r_2,\, a_1,\, a_2,\, \Omega,\, d,\, Re\big). \tag{2.6}$$

The cylinders $\mathcal{C}_\lambda$ and outer boundary $\mathcal{B}$ are assumed disjoint with the $\mathcal{C}_\lambda$ symmetrically placed about the horizontal mid-line of $\mathcal{B}$. Of course, any inherent symmetries of the system should be properly reflected in the determined flow field. In our general numerical code we make no symmetry assumptions: these should emerge as part of the solution and will provide a check of numerical accuracy.

Let $\mathcal{G}$ denote those geometries that are π-rotationally symmetric. The class $\mathcal{G}$ requires the cylinders to be equal and symmetrically placed with respect to the rectangular boundaries (i.e. $r_1 = r_2$, $a_1 = d - a_2$) and there are clearly three independent transformations under which the geometries of $\mathcal{G}$ are unaltered: $\mathcal{R}_1$, a reflection in the vertical axis $x = d/2$; $\mathcal{R}_2$, a reflection in the horizontal axis $y = 0$; $\mathcal{Q}$, a rotation through π about an axis through $(d/2, 0)$ but perpendicular to the plane of the motion. (In fact, the general geometry of Figure 1 is left unaltered under the transformation $\mathcal{R}_2$.) But geometrical invariance for flow symmetry is not sufficient, we also require dynamic invariance. The symmetry class for $Re = 0$ will generally be larger than that for non-vanishing Reynolds numbers. For each of the symmetries above, Table 1 shows the appropriate transformations of the fields ψ and p (from which $\mathbf{u}$ and ω can be deduced) that leave the geometry,

	Geometry $\mathcal{G}$, $\Omega = \pm 1$			General Geometry $\mathcal{T}$
	$\mathcal{R}_1$	$\mathcal{R}_2$	$\mathcal{Q}$	$\mathcal{R}_2$
$Re = 0$	$\psi \to \pm\psi$ $p \to \mp p$	$\psi \to \psi$ $p \to -p$	$\psi \to \pm\psi$ $p \to \pm p$	$\psi \to \psi$ $p \to -p$
$Re \neq 0$ $(\Omega = 1)$	——	——	$\psi \to \psi$ $p \to p$	——
$Re \neq 0$ $(\Omega = -1)$	$\psi \to -\psi$ $p \to p$	——	——	——

Table 1: Symmetries for triply-connected Taylor–Couette system

governing equations and boundary conditions unaltered. We see immediately that, if the cylinders co-rotate in geometry $\mathcal{G}$ at equal speeds ($\Omega = 1$), then the constants c_1 and c_2 must be equal. Similarly, in the case of equal counter-rotation ($\Omega = -1$) for $\mathcal{G}$, we must have $c_1 = -c_2$.

Koh [20] considered the case of co-rotating cylinders in the square geometry $\mathcal{G}_1$ [see (2.7)] with rotation ratio $\Omega = 1$ and obtained their solution by imposing a quarter-box symmetry. While it is clear from Table 1 that the assumption is indeed valid for inertia-less flows, it is not correct for $Re \neq 0$ and as a consequence their solutions are flawed.

Experimental investigations (including our own in §5) have concentrated on the symmetric geometries $\mathcal{G}$. Although the theoretical discussions of this paper are general, the particular numerical results relate to the specific configurations $\mathcal{G}_1$ and $\mathcal{G}_2$,

$$\textbf{Square geom. } \boldsymbol{\mathcal{G}_1}\text{: } r_1 = 0.25, \quad r_2 = 0.25, \quad a_1 = 0.6, \quad a_2 = 1.4, \quad d = 2.0, \tag{2.7a}$$

$$\textbf{Rectangular geom. } \boldsymbol{\mathcal{G}_2}\text{: } r_1 = 0.5, \quad r_2 = 0.5, \quad a_1 = 1.0, \quad a_2 = 2.5, \quad d = 3.5, \tag{2.7b}$$

which exemplify the flow patterns of the triply-connected geometry. The configuration $\mathcal{G}_1$ directly relates to the experiments of Vladimirov [16]. The experiments of Carlotti [14] and those described in §5 have the $\mathcal{G}_1$ domain size and cylinder positions but employ slightly smaller cylinders ($r_1 = r_2 = 0.2$). The geometry $\mathcal{G}_2$ involves a more elongated container with the cylinders occupying half the height of the box.

2.3. The numerical solution

(a) Numerical scheme

To solve (2.3a) and (2.4) with (2.5) we use a multi-level iterative scheme. To accommodate the fluid inertia we first determine by numerical means the stream-function and vorticity field appropriate to the Stokes approximation of negligible

inertia ($Re = 0$). This solution is then used to initiate the case when the effects of inertia first become significant ($Re \ll 1$). Solutions for larger values of Re are successively determined in the same manner using the previous solutions as a starting point. The general method is based on a standard finite difference scheme and is capable of addressing independent variations in the seven-dimensional parameter space (2.6). To allow a flexibility to accommodate small cylinder–cylinder and cylinder–wall gaps the number of grid-lines in different regions is independently variable. We show in Figure 2 the details of the five grid parameters $(n_1, n_2, n_3, m_1, m_2)$ used across the full domain. The underlying grid is Cartesian so as to accommodate easily the boundary $\mathcal{B}$ and n_κ and m_μ respectively denote the number of vertical and horizontal grid lines in a region. But, due to the presence of the cylinders $\mathcal{C}_\lambda$, we must take particular care in specifying the grid-line intervals.

Above all, we wish to avoid interpolation at the circular boundaries and therefore seek to arrange for grid points to lie on these boundaries. As a consequence, our grid must be unevenly spaced in both the horizontal and vertical directions since whenever a vertical grid line crosses a boundary there will need to be a corresponding horizontal grid line and *vice versa*. However, positioning nodes on a cylindrical boundary is delicate: if the nodes are chosen at equal intervals around the boundary in the manner of a polar system or simplistically at even intervals along one axis, there is a bunching of grid-lines. Grid-line bunching can cause numerical difficulties and can be a factor in uneven or failed convergence. It was found that, by choosing nodes at the left and right extremities of the $\mathcal{C}_\lambda$ by the intersection of equally spaced vertical grid-lines, and nodes at the top and bottom of the cylinders by the intersection of equally spaced horizontal grid-lines, cylinder induced grid-line bunching could be largely avoided. The grid spacing in those regions where the horizontal and vertical grid-lines do not intersect $\mathcal{C}_\lambda$ also requires attention to avoid sharp changes in grid-line spacing. The number of grid-lines in these regions are specified independently and we introduce a linear variation in the spacing so that the grid-line interval employed at the cylinder edges is gradually increased (or decreased) at a constant rate towards the boundary $\mathcal{B}$. It was found that both these grid-features considerably improved the performance of our numerical scheme: convergence was achieved in fewer iterations and numerical 'noise' was reduced. The even vertical grid-line spacing at the top and horizontal grid-line spacing at the left of a cylinder is illustrated in Figure 3 together with the linearly increasing spacing towards the outer rectangle.

The discretised set of equations for determining the streamfunction and vorticity are obtained by second-order central finite differences. However, the uneven grid means that, for our system to be truly second order, more remote nodes will be required than for an evenly spaced grid. To illustrate, recall that the familiar uniform grid central difference formula $\chi_{xx}(x) = [\chi(x+h) - 2\chi(x) + \chi(x-h)]\, h^{-2}$ with error $\mathcal{O}(h^2)$ can be established using Taylor expansions about the centre point. The uniform spacing, h, between the three points involved means that

the combination on the right-hand side does not involve the derivatives χ_x, χ_{xxx}. Evidently, when the grid point spacing is non-uniform, such cancellations will not simultaneously occur. Essentially, to eliminate both derivatives χ_x and χ_{xxx} and so obtain an equivalent second order formula for a non-uniform grid, more distant nodes and their associated Taylor expansions are needed. Although the resulting approximations are more cumbersome, the process is nevertheless quite straightforward. Kantorovich [23] (see pages 180, 200ff) demonstrate the technique to determine second order derivatives over an uneven net and discuss the order of the remainder generated.

The resulting system of equations for the ψ- and ω-arrays are solved using successive over relaxation (SOR). Essentially, at a given Reynolds number, one of the arrays is held fixed, the other repeatedly updated until a recognisable convergence occurs and then the rôles of the two arrays are reversed. The procedure continues until there is convergence to a simultaneous solution for both arrays at every grid point. To begin the process for the case $Re = 0$ we use zero arrays for both ψ and ω. For non-vanishing Re we use the previous solution for ψ and ω as a starting point. The SOR method can be slow but benefits from the considerable advantages of being easy to implement and, in the present application at least, its robustness to variations in the parameter space.

Off-centre second-order finite differences must be used as we approach a boundary and it is clearly necessary to specify the values of the streamfunction and vorticity at boundary nodes. The values of the streamfunction on the cylinder are determined by a root search using the condition (2.5). The grid boundary values of the vorticity are determined from (2.3a) in a straightforward manner using Taylor expansions of ψ at neighbouring points to the boundaries. During the early stages of relaxation when we must initiate the ψ and ω fields with values from a previous iteration, the values of the streamfunction and vorticity which we enforce through the conditions above can result in (temporary) extreme gradients. Therefore, to accommodate any dramatic physical or numerical jumps we include a smoothing parameter, γ (< 1), applied to the vorticity array at the boundaries that acts somewhat like the usual SOR relaxation parameter: at each iteration, the value of ω is increased by γ multiplied by the increase implied by the Taylor expansion. By this process the flow adapts gradually to the new boundary conditions. Our code progressively reduces the magnitude of γ after the early stages of relaxation.

(b) Numerical checks

Given any point in the seven-dimensional parameter space (2.6), the scheme for determining the streamfunction ψ and vorticity ω of the two-roll mill also requires the grid parameters depicted in Figure 2 and the relaxation parameters associated with the iterative process. As a matter of routine all the solutions we obtained were tested for consistency under variations of both sets of parameters and the contour of condition (2.5). Contours could encompass one or both cylinders, thus demonstrating that not only was the numerical integration independent of the path taken but also our choice of c_λ's were physically realisable.

The functions ψ and ω were only judged to have been determined if the change in both with successive iterations was less than 10^{-6}. In addition, by monitoring the differences $\nabla^2\omega - Re(\mathbf{u}.\boldsymbol{\nabla})\omega$ and $\nabla^2\psi - \omega$ at each node, the governing equations [see (2.3a) and above] were shown to be satisfied to within a tolerance of 10^{-5}.

Confidence in the overall numerical scheme is founded on three additional considerations. First, the procedures were tested on a single rotating cylinder in a square box. This problem has been discussed by Lewis [5] using symmetry arguments to interpolate from the quarter box geometry and a different set of criteria for grid placement. Using the whole flow domain, we recovered all the essential flow features and numerical values reported by Lewis [5] and our scheme has some advantages: fewer iterations are needed; deviations in $\nabla^2\omega$ for $Re = 0$ are reduced and confined to a small neighbourhood; point-wise fluid velocities on the cylinders are quickly found to within 1% of their theoretical value. Second, for the two-roll mill, although no *a priori* symmetry was imposed in our code, the solutions we obtained were all in concert with the theoretical results of Table 1. Our final check relates to the boundary condition on the cylinders $\mathcal{C}_\lambda$. The numerically determined solution provides, via $\nabla\psi$, values for the fluid velocity on $\mathcal{C}_\lambda$ which can be directly compared with the conditions (2.3b). Thus these velocity boundary conditions are not abandoned but provide us with an important pointwise check on our solutions. In addition the cylinder circulations, considered as an alternative to equation (2.5), were verified.

3. Basic flow characteristics of a two-roll mill

Physically the flows associated with co- and counter-rotation are so different that it is necessary to treat these cases separately. To elucidate predominant features we will concentrate in this section on the square and rectangular geometries $\mathcal{G}_1$ and $\mathcal{G}_2$ [see (2.7)] with rotation ratios ± 1. In the next section we shall consider the symmetry-breaking cases in which the rotation ratio lies in the range $(-1, +1)$, corresponding to slow equilibrium transitions between the two extreme cases of this Section.

The experimental work of Vladimirov [16], Carlotti [14] and that reported in §5 show that, for the square geometry $\mathcal{G}_1$, the two-dimensional base flow relating to co-rotating cylinders becomes unstable to three-dimensional disturbances for Reynolds numbers $Re_{\text{crit}} \gtrsim 209.2$. These studies provide us with an idea of the range of Reynolds numbers, Re, we should investigate for the two-dimensional flows. It does not necessarily follow, however, that beyond the experimentally determined critical Reynolds number the unperturbed solution no longer exists: it may be that physically a bifurcation to a second solution has occurred. Numerical methods arrive at a solution by iteration and inevitably impose random disturbances on the true solution. But these disturbances need not be of the sort that promote the physically observed instability. The numerical solution can often be pursued for Reynolds numbers beyond Re_{crit}. For example, by exploiting sym-

metry, Lewis [5] produced numerical solutions for the single-cylinder geometry with Re values well beyond the experimentally observed $Re_{\rm crit}$. The experiments described in Section 5 confirm the Vladimirov critical value for co-rotating cylinders but numerically we have been able to determine a two-dimensional solution for a Reynolds number as large as 400. There need not be any inconsistency – either our assumption of a steady flow or the assumption of a two-dimensional flow becomes physically unrealistic at higher Re. In practice we continued to increase Re until it became numerically impractical due to either the size of increment in Re or the degree of smoothing required.

3.1. Co-rotating cylinders ($\Omega = 1$)

A. The basic flow within the square geometry $\mathcal{G}_1$

We begin by concentrating on the geometry $\mathcal{G}_1$ in which the diameters of the (equal) cylinders are a quarter of the height of the square box. The cylinders are co-rotating with the same angular speed. The streamlines and iso-vorticity contours for the case of vanishing inertia were determined using grid parameters $n_1 = n_2 = n_3 = m_2 = 30$, $m_1 = 20$ (see Figure 2) and are illustrated in Figure 4. The symmetries anticipated in Table 1 are all present and the character of the flow is dominated by two special streamlines, namely, the streamline separatrix, $\Psi_{\rm X}$, passing through the saddle point at (1,0) and the separation streamline $\Psi_{\rm S}$, corresponding to $\psi = 0$ that intersects the vertical sides of the bounding box. The separatrix $\Psi_{\rm X}$ has value $\psi = -1.09$E-1 while on $\mathcal{C}_\lambda$ the streamfunction takes values $c_1 = c_2 = -1.77$E-1. In Figure 4 the set of contour values of the plot are: $\psi = [1.\text{E-}3, 1.\text{E-}4, 0, -2.\text{E-}3, -1.\text{E-}2, -3.\text{E-}2, -6.5\text{E-}2, -1.09\text{E-}1, -1.4\text{E-}1]$, $\omega = [0.2, 0, -0.2, -0.5, -1, -1.5, -2.25, -3, -4, -5.5]$.

The fluid inside the separatrix is confined to the neighbourhood of each cylinder and rotates in an almost circular fashion, while outside $\Psi_{\rm X}$ the fluid moves along streamlines which encompass both cylinders. The flow on either side of the separation streamline $\Psi_{\rm S}$ moves in opposite senses. Since the flow is steady, $\Psi_{\rm S}$ is also a particle path but, because the streamline intersects the stationary bounding surface $\mathcal{B}$, a particle will take infinite time to travel along this contour. At the top and bottom of the box, beyond $\Psi_{\rm S}$, there are regions of re-circulation, where the fluid velocity is considerably weaker than in the main flow.

The extent to which the symmetries of Figure 4 relate to the neglect of fluid inertia in (2.3a) can be judged by comparison with Figures 5(*a,b*) based on the same grid parameters. The two values of the Reynolds number ($Re = 150$, 400) are chosen to be representative of intermediate values, $Re \in (0, 400)$. The figures possess a π-rotational symmetry but we observe that as Re increases the re-circulation region grows in size and there is also a general skewing of the flow in the anti-clockwise direction. (Recall that both cylinders are rotating in an anti-clockwise fashion with unit velocity.) Perhaps the skewing is most easily monitored by the intersection of $\Psi_{\rm S}$ with the vertical boundaries of $\mathcal{B}$. The respective separatrices $\Psi_{\rm X}$ have values $\psi = -1.15$E-1, $\psi = -1.22$E-1 and the associated

streamfunctions on $\mathcal{C}_\lambda$ are *a*) $c_1 = c_2 = -1.78\text{E-}1$, *b*) $c_1 = c_2 = -1.76\text{E-}1$. Interestingly the angle Ψ_X forms at $(1, 0)$ remains between 56° and 60° as Re increases from 0 to 400. We found that the size and intensity of the recirculations increased monotonically with Re. The tendency to skew however increased up to $Re \sim 200$, after which it gradually declined. The streamfunction illustrated in Figure 5 corresponds to the sets: *a*) $\psi = [1.\text{E-}3, 0, -2.\text{E-}3, -1.\text{E-}2, -3.\text{E-}2, -6.7\text{E-}2, -1.15\text{E-}1, -1.4\text{E-}1]$; *b*) $\psi = [4.1\text{E-}3, 3.5\text{E-}3, 2.5\text{E-}3, 0, -1.\text{E-}2, -3.\text{E-}2, -6.7\text{E-}2, -1.22\text{E-}1, -1.5\text{E-}1]$.

The vorticity diagrams of Figure 5 for respective contour values *a*) $\omega = [0.5, 0, -0.5, -1, -1.22, -2, -3, -5]$, *b*) $\omega = [1, 0, -0.5, -1, -1.27, -2.5, -6]$, show that, as the fluid inertia increases, the iso-vorticity contours become more and more wrapped around the cylinders. This phenomenon is also observed for the single cylinder (see [5]). There, the vorticity contours eventually form closed loops around the cylinder indicating regions of almost constant vorticity. It is possible that the contour deformation may be the early manifestation of the Prandtl–Batchelor theorem for these particular geometries. For two-dimensional bounded flows the Prandtl–Batchelor theorem (see [24]) shows that, in the limit $Re \to \infty$, viscosity is effectively confined to thin boundary layers and that vorticity is constant between these layers. Chipman [25] have applied the Prandtl–Batchelor theorem to the geometry of a single cylinder, eccentrically placed in a circular domain, to find a numerical solution for the streamfunction in the high Reynolds number limit. The Prandtl–Batchelor limit for the triply-connected geometry would imply three regions of constant vorticity – one outside the separatrix Ψ_X and one inside each lobe of the figure-of-eight streamline.

B. The basic flow within the rectangular geometry $\mathcal{G}_2$

To investigate the influence of container shape and relative cylinder size on the flow within a two-roll mill we next consider the geometry $\mathcal{G}_2$ where the cylinders occupy half the height of the domain with aspect ratio $(2 : 3.5)$. Figure 6 is constructed using grid parameters $n_\kappa = m_\mu = 25$ $(\kappa = 1, 2, 3,\ \mu = 1, 2)$ and Figure 6(a) represents the inertia-less flow which should be compared with Figure 4. Figure 6(b) shows the influence of inertia ($Re = 350$). The values of the streamfunction on the separatrix and cylinder boundaries are *a*) $\psi = -1.21\text{E-}1$, $c_1 = c_2 = -2.36\text{E-}1$ and *b*) $\psi = -1.64\text{E-}1$, $c_1 = c_2 = -2.51\text{E-}1$. The remaining contour values of Figure 6 are *a*) $\psi = [0, -5.\text{E-}3, -2.\text{E-}2, -5.\text{E-}2, -1.21\text{E-}1, -1.7\text{E-}1]$, $\omega = [0, -0.5, -1, -1.25, -2]$, *b*) $\psi = [2.5\text{E-}4, 7.5\text{E-}4, 0, -1.\text{E-}2, -4.\text{E-}2, -1.\text{E-}1, -1.64\text{E-}1, -2.\text{E-}1]$, $\omega = [1, 0, -0.95, -1.15, -1.3, -1.6, -3]$. All the expected symmetries are present, as are several of the flow characteristics found in the $\mathcal{G}_1$ case. In particular, the separatrix-angle is largely insensitive to Re, the recirculation regions skew and intensify with inertia and the iso-vorticity contours are progressively deformed around the cylinders. The most marked difference, however, relates to the re-circulation region. For $\mathcal{G}_2$ the streamline of separation no longer traverses the full box width but appears at the four corners. The recirculation regions take the form of eddies. From the work of Moffatt [26] we know these eddies are the first of a diminishing sequence towards the corner.

Their structure, size and penetration into a general wedge has been more fully described by Hills [27].

The streamfunction provides an insight into mass transport within the various regions of the flow domain. Since the streamfunction vanishes on the boundary, the value of ψ at any point gives a measure of the flux between the boundary and that point. Thus the intensity of the flows can be inferred from the contour values. Generally for both geometries $\mathcal{G}_1$ and $\mathcal{G}_2$ the mass flux increases with Reynolds number. In the case of $\mathcal{G}_1$ and Reynolds numbers in the range $Re \in (200, 400)$ we found a slight decline in flux that is perhaps attributable to the interaction of the main flow with the recirculation regions. The flux in the re-circulation regions is relatively small, between 0.2% and 2% of that in the main flow, but nevertheless increases with Re. The proportion of fluid "trapped" within the separatrix decreases with increasing inertia, a result which is not wholly surprising – as the fluid becomes less viscous the internal friction will drive less neighbouring fluid and the boundary layer formed at a cylinder boundary will thin. Although the total flux and the fluid transported outside the separatrix is greater for $\mathcal{G}_2$ than that for $\mathcal{G}_1$, the proportion of fluid outside the separatrix is greater for the square geometry $\mathcal{G}_1$.

Finally in this subsection we extrapolate the nature of the flow field for geometries other than $\mathcal{G}_1$ and $\mathcal{G}_2$. We have seen that re-circulation regions occur where the rotationally-driven flow has become weak. As we move away from the main flow, cells are formed which circulate in the opposite sense to the main flow. For the square geometry $\mathcal{G}_1$ the flow is weak across the whole width of $\mathcal{B}$, whereas in the more elongated $\mathcal{G}_2$ the flow is only sufficiently weak in the corners. In a geometry formed by stretching $\mathcal{G}_1$ vertically, the original re-circulation region would also weaken and spawn in turn its own re-circulation region (with the same sense as the main flow). In the limit of a tall geometry we would expect a stack of such cells in the vertical direction. Similarly, a box formed by extending the width of the container in $\mathcal{G}_2$ would generate an array of re-circulation cells in the horizontal direction, reminiscent of the reversing cell structure found by Mak [28] in a horizontal channel driven by an external flow across a small gap. We should emphasise, however, the intensity of all such re-circulation regions is likely to be extremely small and may indeed be beyond numerical accuracy.

3.2. Counter-rotating cylinders ($\Omega = -1$)

Co-rotating cylinders set up a shearing motion between the cylinders but in the case of counter-rotation there is, in this region, flow reinforcement. Thus, on physical grounds we must expect the flow character of these two cases to be very different. Figure 7 is based on grid parameters $n_\kappa = m_\mu = 25$ and illustrates for the rectangular geometry $\mathcal{G}_2$ the flow fields produced in a counter-rotating two-roll mill at increasing Reynolds number, $Re = 0, 50, 150$. The contour values in each of the plots are given by: *a*) $\psi = [\pm$1.5E-1, $\pm$5.E-2, $\pm$1.E-2, $0]$, $\omega = [\pm 2, \pm 1, \pm 0.8, \pm 0.5, \pm 0.25, 0]$, $c_1 = -c_2 = -$2.36E-1; *b*) $\psi = [\pm$5.E-2, $\pm$1.E-2,

$\pm$5.E-4, 0], $\omega = [\pm 2.88, \pm 2, \pm 1, \pm 0.2, 0]$, $c_1 = -c_2 = -1.49$E-1; *c*) $\psi = [\pm$3.E-2, $\pm$1.5E-2, $\pm$3.E-3, 0], $\omega = [\pm 4.74, \pm 2.8, \pm 1.3, \pm 0.5, 0]$, $c_1 = -c_2 = -6.84$E-2. We see the expected symmetries listed in Table 1 and there are two sets of streamlines that encircle each cylinder on either side of a separating streamline Ψ_S for which $\psi = 0$. With due allowance for a fluid interface boundary condition on Ψ_S, the flow on either side of the separating streamline resembles that of an isolated cylinder. The flow field for the geometry $\mathcal{G}_1$ is substantially the same.

In Figure 7 the left-hand cylinder rotates counter clockwise so the fluid motion between the cylinders is reinforced in a uniform upward direction. As a consequence, a local Reynolds number based on the fluid speed in this region is larger than elsewhere and we might well expect instabilities to occur here for lower rates of rotation than for co-rotating cylinders. To an extent this observation is borne out by our numerical solution: the maximum practical Reynolds number (based on the cylinder speeds) for this case was less than half the maximum for the co-rotating cylinders. Figure 7(*b*) relates to $Re = 50$ and it is clear that, at this value, the contour $\psi = 0$ has created several new regions of re-circulation (four in each half of the domain) and, when the Reynolds number is increased still further ($Re = 150$, see Figure 7*c*), the separating streamline detaches from the boundary and actually creates a re-circulating cell around the cylinder itself It should be emphasised that the flow in these cells is extremely weak and becomes progressively so as we approach the boundary $\mathcal{B}$. Indeed, it is questionable whether Figures 7(*b*) and 7(*c*) will ever be seen physically before the onset of instability.

We close this section by relating our work to previous results. The study of Koh [20] concerns co-rotating cylinders with $\Omega = 1$ in the square geometry $\mathcal{G}_1$. Their streamline patterns for inertia-less flows are substantially the same as those of Figure 4 but there is a significant difference when inertia effects are included. For this case the Koh [20] plots show no evidence of skewing (a fundamental characteristic of Figure 5). The disparity can be traced to the use of an incorrect boundary condition: their scheme incorrectly imposes a quarter-box symmetry (see §2.2). The study of Price [17] considered the co- and counter-rotation of a two-roll mill confined in a circular boundary for the case of linear creeping flow. His plots exhibit the characteristic recirculation regions and saddle points for co-rotating cylinders, although we would not, of course, expect corner eddies in a circular geometry. Direct comparison with Price [17] is difficult: his streamlines are qualitative not quantitative. Nevertheless it is reassuring to observe that the transitions (see below) and flow characteristics reported by him are present in our flow diagrams relating to inertia-less flow.

4. Two-roll mill flow transitions

The previous section has established the flow characteristics of a bounded two-roll mill for co- and counter-rotation when the cylinders have equal angular speeds. In this section we regard these two cases as end states of a family of

(steady) states obtained by allowing the rotation ratio, Ω, to decrease continuously from 1 (co-rotation) to -1 (counter-rotation). We are interested in the characteristics of the intermediate states, $\Omega \in (-1, 1)$. On physical grounds we expect the flow patterns to deform continuously from one end régime to the other.

The topological features (centres, saddle points and separation points) of the transition states must satisfy the constraint of the Euler characteristic, an invariant of topologically equivalent spaces (see [29]). Generally, if n_c denotes the number of centres, n_s the number of saddle points and n_p the number of separation points of the contours of a continuous field then for our triply-connected domain the Euler characteristic constraint requires

$$n_c - n_s - \tfrac{1}{2}n_p + 1 = 0. \tag{4.1}$$

The streamlines of Figure 6 for example have $n_c = 4$, $n_s = 1$, $n_p = 8$, in accord with (4.1).

Evidently equation (4.1) restricts the flow transitions that may occur: a continuous deformation cannot introduce or remove a saddle-point or centre in isolation, but a centre may be eliminated if two separation points are simultaneously removed; a saddle-point and a centre may similarly cancel each other. As an illustration, let us imagine for the co-rotating case with vanishing inertia a continuous deformation of the geometry $\mathcal{G}_1$ into $\mathcal{G}_2$ (Figures $4a$ and $6a$). We see that the effect of such a deformation is to introduce four new separation points and to remove two centres and four saddle points in the recirculation region, consistent with (4.1). Our interest in this section will be the transitions of the main flow. Of course, the recirculation regions may include many interesting topological features but the flows in these regions are very weak and therefore difficult to resolve accurately. For example, in the theoretical limit, the Moffatt eddies that are seen in the corners of Figure 6 are the first of an infinite cascade towards the corner each with a centre and two additional separation points, but their intensities decay exponentially. We shall therefore only discuss visible streamline topology.

The constraint (4.1) will provide an independent check on the variations $\Omega \in (-1, 1)$. Figure 8 relates to the rectangular geometry $\mathcal{G}_2$ with $Re = 0$ using grid parameters $n_\kappa = m_\mu = 25$. It shows a series of five intermediate states relating to rotation ratios $\Omega = 0.5,\ 0.1,\ 0,\ -0.1,\ -0.5$. Only figures (a), (b) possess separatrices on which $\psi = -8.1\text{E-}2,\ -2.23\text{E-}2$ respectively. In Figure $8(a)$ the special streamline $\psi = -8.15\text{E-}4$ intersects the boundary $\mathcal{C}_2$. Explicitly, the contours relate to the values*: $a)$ $\psi = [-1.7\text{E-}1, -1.1\text{E-}1, -8.1\text{E-}2, -3.\text{E-}2, -3.\text{E-}3, 0, 4.\text{E-}5]$, $c_1 = -2.36\text{E-}1$, $c_2 = -1.19\text{E-}1$; $b)$ $\psi = [-1.5\text{E-}1, -1.\text{E-}1, -5.\text{E-}2, -2.25\text{E-}2, -3.5\text{E-}3, 0, 5.\text{E-}5]$, $c_1 = -2.35\text{E-}1$, $c_2 = -2.43\text{E-}2$; $c)$ $\psi = [-1.5\text{E-}1, -7.\text{E-}2,$

*In the case of inertia-less flows the system is linear and, for symmetric geometries (such as $\mathcal{G}_2$ here), the streamfunction values c_λ can be checked for an arbitrary rotation ratio by the linear superposition of two known solutions.

$-3.E\text{-}2, -5.E\text{-}3, -8.15E\text{-}4, -4.E\text{-}4, 0, 3.E\text{-}4, 8.E\text{-}4]$, $c_1 = -2.35E\text{-}1$, $c_2 = -8.E\text{-}4$; *d*) $\psi = [-1.5E\text{-}1, -7.E\text{-}2, -2.E\text{-}2, 0, 2.E\text{-}3, 1.E\text{-}2]$, $c_1 = -2.35E\text{-}1$, $c_2 = 2.27E\text{-}2$; *e*) $\psi = [-1.3E\text{-}1, -7.E\text{-}2, -2.E\text{-}2, 0, 1.E\text{-}2, 5.E\text{-}2]$, $c_1 = -2.35E\text{-}1$, $c_2 = 1.17E\text{-}1$. In the top left diagram, where the left-hand cylinder moves at twice the speed of the other, the flow pattern has not changed significantly from that of Figure 6. Perhaps the most noticeable difference is that the eddies in the corners are larger on the left-hand wall of $\mathcal{B}$ and the flow around $\mathcal{C}_1$ is more intense. The left-hand cylinder dominates the transport of fluid. As the right-hand cylinder slows to $\Omega = 0.1$ (Figure 8*b*) we observe that, not only has the flow around $\mathcal{C}_2$ become extremely weak, but that two new re-circulation regions have formed in the middle of the top and bottom boundaries. Thus there are now four new separation points and two new centres. In the middle left diagram the cylinder $\mathcal{C}_2$ is at rest. The newly separated regions for $\Omega = 0.1$ have grown but there is still a flow external to both cylinders. Now the saddle-point between the cylinders has been replaced by two separation points on $\mathcal{C}_2$. Once the cylinders are counter-rotating (Figure 8*d*) the two new re-circulations coalesce and enclose the right-hand cylinder. As Ω decreases to -0.5 (bottom plot) the circulation around the right-hand cylinder increases in intensity and the flow has taken on the characteristics of the counter-rotating case.

We have seen in the previous section that fluid inertia skews the flow patterns of $Re = 0$ flows. Yet another manifestation of this phenomenon is observed in the plots of Figure 9 that relates to the rectangular geometry $\mathcal{G}_2$ and grid parameters $n_\kappa = m_\mu = 25$ with rotation ratio 0.5. The Reynolds numbers and contour values are given by: *a*) $Re = 100$, $\psi = [-1.6E\text{-}1, -1.15E\text{-}1, -9.18E\text{-}2, -5.E\text{-}2, -7.5E\text{-}3, 0, 2.E\text{-}4]$; *b*) $Re = 137$, $\psi = [-1.7E\text{-}1, -1.15E\text{-}1, -9.24E\text{-}2, -5.E\text{-}2, -8.E\text{-}3, 0, 2.E\text{-}3, 4.E\text{-}3]$. The corresponding streamfunction value on the separatrix and the $\mathcal{C}_\lambda$'s are *a*) $\psi = -9.18E\text{-}2$, $c_1 = -2.19E\text{-}1$, $c_2 = -1.36E\text{-}10$, *b*)$\psi = -9.24E\text{-}2$, $c_1 = -1.44E\text{-}1$, $c_2 = -2.42E\text{-}1$. Comparing with Figure 8(*a*) we see that, in addition to the skewing, the re-circulating corner eddies on the left-hand boundary have become significantly larger. More interesting, however, is the appearance of a new re-circulation region, created by the introduction of two new separation points and a centre near the bottom boundary. As the Reynolds number increases further to $Re = 137$ (Figure 9*b*), the middle-bottom and left separation regions prepare to detach to form one region. In addition, as Re increases the flux due to the slower cylinder ($\mathcal{C}_2$ with $\psi = c_2$) increases steadily whilst the boundary streamfunction value for $\mathcal{C}_1$ decreases. At a Reynolds number of between 120 and 130 the cylinder with the dominant flux swaps so that at a $Re = 137$ (Figure 9*b*) the majority of the streamlines now surround the right-hand cylinder. This is a slightly surprising result. It is possible that the growing re-circulation region inhibits the flux due to the left-hand cylinder. But there is another explanation. The Reynolds number we have used is based on the angular velocity of cylinder $\mathcal{C}_1$. Were we to employ two independent local Reynolds numbers based respectively on the angular velocities Ω_1 and Ω_2, then the Reynolds number of the left-hand cylinder would be the larger. Therefore, if

the flow around the cylinders is regarded as contained within a boundary layer, this layer would be thinner for the left-hand cylinder so reducing the fluid transport. Of course, two-dimensional flows with $Re > 120$ may not be physically attainable before the onset of instability and such considerations may not arise.

In the inertia-less flow of Figure $8(c)$, the right-hand cylinder is stationary but the streamfunction is non-zero on $\mathcal{C}_2$. In fact, we have seen that $c_2 = -8.\text{E-}4$ and there is still a small circulation external to both cylinders. The saddle point has also become degenerate. However, as the Reynolds number increases to $Re = 17.4$ with $\Omega = 0$ (shown in Figure $10a$), the streamline constant c_2 tends to zero and the right-hand cylinder lies on the separation streamline formed by joining the top and bottom re-circulation regions. As Re increases further ($Re = 40$, Figure $10b$) the right-hand cylinder is totally enclosed in a re-circulation region and the flow becomes similar in appearance to the streamline pattern for slowly counter-rotating cylinders. The full set of contour values shown in Figure 10 are:
$a)$ $\psi = [-1.\text{E-}1, -3.\text{E-}2, -5.\text{E-}3, 0, 2.\text{E-}4, 1.\text{E-}3, 1.5\text{E-}3]$, $c_1 = -2.36\text{E-}1$, $c_2 = 0$;
$b)$ $\psi = [-1.6\text{E-}1, -7.\text{E-}2, -3\text{E-}2, -5.\text{E-}3, 0, 2.\text{E-}3, 1.\text{E-}3, 1.\text{E-}4, 3.\text{E-}3]$,
$c_1 = -2.39\text{E-}1$, $c_2 = 1.9\text{E-}3$.

It is interesting to compare the results of this Section with the earlier, unpublished, work of Price [19]. For the same geometry as his previous experimental investigation with a circular outer boundary he considers the Stokes flow found numerically by using a series expansion in the complex plane, incorporating point vortices at the centres of the cylinders. He calculates the streamfunctions ψ_1 and ψ_{-1} corresponding to equally co-rotating and counter-rotating cylinders respectively. The fixed symmetry of his domain then allows him write the general solution for arbitrary rotation ratio Ω as $\frac{1}{2}\left[(1+\Omega)\psi_1 + (1-\Omega)\psi_{-1}\right]$. Exploiting symmetries possessed by Stokes flows he computes the streamfunctions over the quarter domain for 152 terms. Price [19] then analyses the flow transitions that occur for his geometry as Ω tends from 1 to -1, making use, as we have done, of the Euler characteristic of the domain. Although due account must be taken of the change in outer boundary shape, the streamline transitions of the main flow are in keeping with those we have found in the inertia-less case.

5. Comparison with experiments

Although a two-roll mill is simple to investigate experimentally, there have been surprisingly few studies especially when compared to the data compiled for single cylinder Taylor-Couette flows and even the four-roll mill configuration. The original two-roll mill experiments of Tarada [15] were part of a much wider study and focused on the manner of the primary instability. More recently there has been the investigations of Carlotti [14] and Vladimirov [16] but since both these studies are in report form only, we present here preliminary results of a predominantly qualitative investigation carried out at the DAMTP Fluid Dynamics Laboratory in Cambridge. The purpose of our experiments was to test the pre-

dictions of the previous sections and, to this end, we have largely concentrated on the two-dimensional flow before the advent of any instability.

The apparatus we used was previously employed by Carlotti [14]. It comprises a 50cm×10cm×10cm perspex box in which two cylinders of radii 1 cm are placed vertically, their centres lying symmetrically on the mid-line of the cross section in the manner of the geometries $\mathcal{G}_1$ and $\mathcal{G}_2$ [see (2.7)]. In the notation of the previous section, the configuration $\mathcal{E}$ (closely related to our 'numerical' geometry $\mathcal{G}_1$) is defined by

$$\textbf{Geometry } \boldsymbol{\mathcal{E}}\text{: } r_1 = 0.2, \quad r_2 = 0.2, \quad a_1 = 0.6, \quad a_2 = 1.4, \quad d = 2.0. \qquad (5.1)$$

To facilitate a suitable range of Reynolds numbers $(0, \sim 200)$ at modest rotation rates, we used glycerine mixed with water at concentrations between 70% and 100% as the contained fluid. The flow structure was illuminated by means of a horizontal light sheet, approximately 2mm thick and the photographs taken by a camera sited below, using natural pearl essence to reveal the streamlines. To minimise end effects the light sheet was placed between 20 and 30cm above the base of the container. (Near the base eddies can be introduced associated with the homogeneous eigensolutions for the geometry that will destroy planar flow – see Hills [30]).

Figure 11 illustrates the flow patterns we obtained for co- and counter-rotation of the cylinders for a variety of Reynolds numbers. In Figure 11(a), which relates to $Re = 1.67$, $\Omega = 1$, the flow is evidently slow and the saddle point, streamline separatrix and symmetries are all clearly visible. The darker region towards the square boundary delineates the separating streamline. The region of re-circulation, therefore, extends the whole width of the box, as depicted in Figures 4 and 5. The longer streaks in Figure 11(b) made by the reflective particles in the glycerine indicate that the fluid is moving much faster. The Reynolds number in this case is 150. The saddle point is clearly present and although the re-circulation regions have grown they still occupy the full box width. There is, however, now a discernible deviation from symmetry: comparison with Figure 11(a) reveals a skewing of the streamlines as predicted above (observe the intersection of these lines with the left-hand and right-hand walls).

Photographs 11(c) and 11(d) relate to low Reynolds number flow ($Re = 1.67$). In the former the rotation ratio is $\Omega = 1/2$ and the figure demonstrates the flux dominance of the faster-moving right-hand cylinder. The predicted flow pattern for this case is set out in Figure 7a. For counter-rotating cylinders, $\Omega = -1$, we see in Figure 11(d) that the flow is contained in two cells surrounding each cylinder (cf. Figure 8a). Also faintly visible at the corners are the beginnings of cascades of eddies described by Moffatt [26].

Finally, we include for completeness Figure 12 which depicts the advent of the primary instability of our two-roll mill. The cell-like structure becomes visible at a Reynolds number $Re \simeq 200$. To obtain these pictures we used a vertical light sheet and photographed the system looking horizontally. The first (Figure 12a) is

taken from a direction passing through both the cylinders axes. Thus, the second cylinder lies behind the first and our light sheet is just in front of the nearest cylinder. The photograph shown in Figure 12(b) relates to a horizontal direction perpendicular to that of the previous case. The cell-like structure surrounding each cylinder is clearly visible, reminiscent of the Taylor cells for a single cylinder, but there is evidence that the cells overlap and even interlock.

Acknowledgements

I would like to thank my thesis advisor, Professor H.K. Moffatt FRS, for his support and many useful insights relating to this work. In addition, I am very grateful to Professor Tom Mullin for his helpful comments and suggestions. My research was funded by EPSRC, U.K.

References

1. G. Stokes, On the theories of the internal friction of fluids in motion and of the equilibrium and motion of elastic solids, *Trans. Camb. Phil. Soc.*, **8**, (1845). 287–319.

2. M. Couette, Etudes sur le frottement des liquides, *Ann. Chim. Phys.*, **21**, (1890). 433–510.

3. G. I. Taylor, Stability of a viscous liquid contained between two rotating cylinders, *Phil. Trans. Roy. Soc. London A*, **223**, (1923). 289–343.

4. M. R. Schumack, W. W. Schultz, and J. P. Boyd, Taylor vortices between elliptical cylinders, *Phys. Fluids A*, **4**, (1992). 2578–2581.

5. E. Lewis, Steady flow between a rotating circular cylinder and a fixed square cylinder, *J. Fluid Mech.*, **95**, (1979). 497–513.

6. M. Hellou, and M. Coutanceau, Cellular flow induced by rotation of a cylinder in a closed channel, *J. Fluid Mech.*, **236**, (1992). 557–577.

7. T. Mullin, and A. Lorenzen, Bifurcation phenomena in flows between a rotating circular cylinder and a stationary square outer cylinder, *J. Fluid Mech.*, **157**, (1985). 289–303.

8. B. Y. Ballal, and R. S. Rivlin, Flow of a Newtonian fluid between eccentric rotating cylinders: inertial effects, *Arch. Rat. Mech. Anal.*, **62**, (1976). 237–294.

9. R. C. DiPrima, and J. T. Stuart, Flow between eccentric rotating cylinders, *J. Lubr. Tech. (ASME)*, **94**, (1972). 266–274.

10. R. C. DiPrima, and J. T. Stuart, Non-local effects in the stability of flow between eccentric rotating cylinders, *J. Fluid Mech.*, **54**, (1972). 393–415.

11. G. Jeffery, The rotation of two circular cylinders in a viscous fluid, *Proc. Roy. Soc. London A*, **101**, (1922). 169–174.

12. E. J. Watson, The rotation of two circular cylinders in a viscous fluid, *Mathematika*, **42**, (1995). 105–126.

13. E. J. Watson, Slow viscous flow past two rotating cylinders, *Q. J. Mech. Appl. Math.*, **49**, (1996). 195–216.

14. P. Carlotti, and S. Obled, *Ecoulements autour de deux cylindres en rotation*, Projet de l'Ecole Polytecnique, (1996).

15. T. Tarada, and K. Hattori, Some experiments on motions of fluids, Part IV, *Rep. Aero. Res. Inst. , Tokyo*, **II**, 26 (1926). 287–326.

16. V. A. Vladimirov, H. K. Moffatt, P. V. Denissenko, and K. I. Ilin, *Report on experimental study of a three-dimensional flow produced by two co-rotating cylinders*, Private communication, (1998).

17. T. J. Price, *Experiments on nonlinear flows in triply-connected systems*, D.Phil. Thesis, University of Oxford, (1991).

18. T. Mullin, Disordered fluid motion in a small closed system, *Physica D*, **62**, (1993). 192–201.

19. T. J. Price, *Numerical characterisation of a family of two roll mill flows*, Private communication, (1994).

20. I. Koh, and J. Chasnov, *Report on a numerical method for computing the steady two-dimensional flow caused by two rotating circles in a rectangle*, Private communication, (1997).

21. G. Harrison, J. Remmelgas, and L. Leal, Comparison of dumbell-based theory and experiment for a dilute polymer solution in a co-rotating two-roll mill, *J. Rheol.*, **43**, (1999). 197–218.

22. P. Singh, and L. Leal, Computational studies of the FENE dumbell model with conformation-dependent friction in a co-rotating two-roll mill, *J. Non-Newton. Fluid Mech.*, **67**, (1996). 137–178.

23. L. Kantorovich, and V. Krylov, *Approximate methods of higher analysis*, translated by Curtis Benster P. Noordhoff Ltd, (1958). 180, 200ff

24. G. K. Batchelor, On steady laminar flow with closed streamlines at large Reynolds number, *J. Fluid Mech.*, **1**, (1956). 177–190.

25. P. D. Chipman, and P. W. Duck, On the high-Reynolds-number flow between non-coaxial rotating cylinders, *Q. J. Mech. Appl. Math.*, **46**, (1993). 163–191.

26. H. K. Moffatt, Viscous and resistive eddies near a sharp corner, *J. Fluid Mech.*, **18**, (1964). 1–18.

27. C. P. Hills, Viscous flow in a wedge produced by a scraping boundary, *Theor. Comp. Fluid Dyn.*, **14**, (2001).

28. V. Mak, and H. K. Moffatt, *Three-dimensional Stokes flow between two parallel plates and near a sharp corner*, Private communication, (1997).

29. J. Milnor, *Morse Theory*, Princeton University Press, (1963). 28–32.

30. C. P. Hills, Eddies induced in cylindrical containers by a rotating end-wall, *Phys. Fluids*, **13**, (2001). 2279–2286.

Figure captions

Figure 1. A representation of the triply-connected geometry of a two-roll mill consisting of two differentially-rotating cylinders $\mathcal{C}_1, \mathcal{C}_2$, with respective radii r'_1, r'_2 in a rectangular domain, $\mathcal{B}$, of dimensions $d' \times 2L'$.

Figure 2. The grid partition of the two-roll mill configuration. The n_κ and m_μ respectively denote the number of vertical and horizontal grid lines in a region. The partition is capable of dealing with small cylinder-cylinder and cylinder-wall gaps.

Figure 3. An illustration of the grid pattern in the neighbourhood of the upper quadrant of a cylinder $\mathcal{C}_\lambda$. It is arranged for a vertical grid-line always to pass through an intersection of a horizontal grid line with a cylinder and *vice versa*. The node distribution has equal y-spacing at the top of the cylinder, equal x-spacing at the left of the cylinder and an adaptive spacing elsewhere (see §2.3*a*).

Figure 4. The streamlines (left) and vorticity contours (right) of the Stokes flow in a two-roll mill within the square geometry $\mathcal{G}_1$ [see (2.7)]. The cylinders are co-rotating counter-clockwise with the same angular speed ($\Omega = 1$). The streamline pattern is dominated by a figure-of-eight separatrix, $\Psi_{\rm X}$, and a separation streamline that delineates recirculations region at the top and bottom of the container from the main flow.

Figure 5. The effects of fluid inertia on the streamlines (left) and vorticity contours (right) of the co-rotating two-roll mill with square geometry $\mathcal{G}_1$ and $\Omega = 1$. The representative cases illustrated are for *a*) $Re = 150$, *b*) $Re = 400$. The inertia has caused the re-circulation regions to grow, the contours to become skewed counter-clockwise and the vorticity within the mill to be intensified.

Figure 6. The influence of the rectangular geometry $\mathcal{G}_2$ [see (2.7)] on the flows of a two-roll mill. The cylinders are co-rotating counter-clockwise with the same angular speed ($\Omega = 1$). The streamlines (left) and vorticity contours (right) are shown for *a*) $Re = 0$, *b*) $Re = 350$. The streamline pattern is again dominated by a figure-of-eight separatrix but now the re-circulation regions are confined to the corners. Non-vanishing inertia causes these regions to grow, skews the flow contours and intensifies the vorticity.

Figure 7. The streamlines (left) and vorticity contours (right) of a counter-rotating two-roll mill with rectangular geometry $\mathcal{G}_2$. The angular speeds of the cylinders are the same ($\Omega = -1$) and the illustrated flow patterns are for Reynolds numbers *a*) $Re = 0$, *b*) $Re = 50$, *c*) $Re = 150$. The flow patterns resemble those of two single cylinders separated by a vertical portion of the streamline $\psi = 0$. This streamline also marks out re-circulation regions at the four corners. With increasing inertia the weak re-circulation regions grow and enclose the cylinders.

Figure 8. The sequence of plots illustrates the continuous deformation of the Stokes flow streamline pattern in geometry $\mathcal{G}_2$ as the rotation ratio Ω is varied between the extremes of co- ($\Omega = 1$) and counter-rotating ($\Omega = -1$) cylinders. The rotation ratios shown are *a*) $\Omega = 0.5$, *b*) $\Omega = 0.1$, *c*) $\Omega = 0$, *d*) $\Omega = -0.1$, *e*) $\Omega = -0.5$.

Figure 9. The effects of inertia on the streamline pattern of a differentially rotating two-roll mill in geometry $\mathcal{G}_2$ with rotation ratio $\Omega = 0.5$ and Reynolds numbers *a*) $Re = 100$, *b*) $Re = 137$. As the Reynolds number increases re-circulation regions migrate away from the rectangular boundary and the flow skews with the slower (right-hand) cylinder eventually dominating mass transport.

Figure 10. A two-roll mill in geometry $\mathcal{G}_2$ in which the right-hand cylinder remains static ($\Omega = 0$). Figure (*a*) illustrates the case $Re = 17.4$ and (*b*) $Re = 40$. In (*a*) the boundary of the stationary cylinder coincides with the streamline of separation ($\psi = 0$) so $c_2 = 0$. As Reynolds number increases ($Re = 40$ and $c_2 = 1.9\text{E-}3$) the flow begins to resemble counter-rotating cylinders.

Figure 11. Photographs of a two-roll mill experiment in the square geometry $\mathcal{E}$ [see (5.1)] using diluted glycerine as the contained fluid. Figures (*a*)–(*c*) relate to co-rotating cylinders with respective rotation ratios and Reynolds numbers *a*) $\Omega = 1$, $Re = 1.67$; *b*) $\Omega = 1$, $Re = 150$; *c*) $\Omega = 0.5$, $Re = 1.67$. The separatrix and re-circulation regions are clearly visible. Case (*d*) relates to counter-rotating cylinders, $\Omega = -1$, at $Re = 1.67$ and shows the separating streamline between the cylinders.

Figure 12. Photographs showing the advent of the primary instability with Taylor cell structure of the co-rotating two-roll mill in the square geometry $\mathcal{E}$ with $\Omega = 1$. The instability occurs at Reynolds number $Re \sim 200$. Figure (*a*) is a side view of the system, while photograph (*b*) is taken from the front.

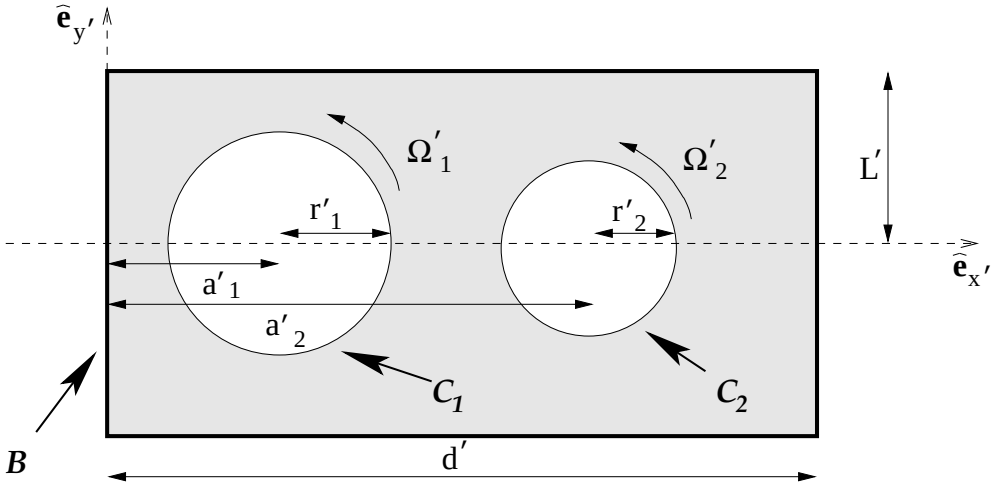

Figure 1:

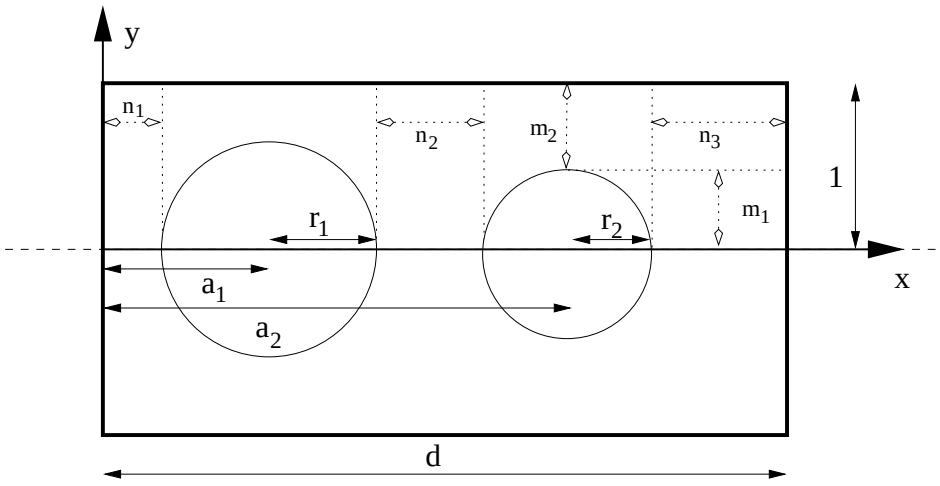

Figure 2:

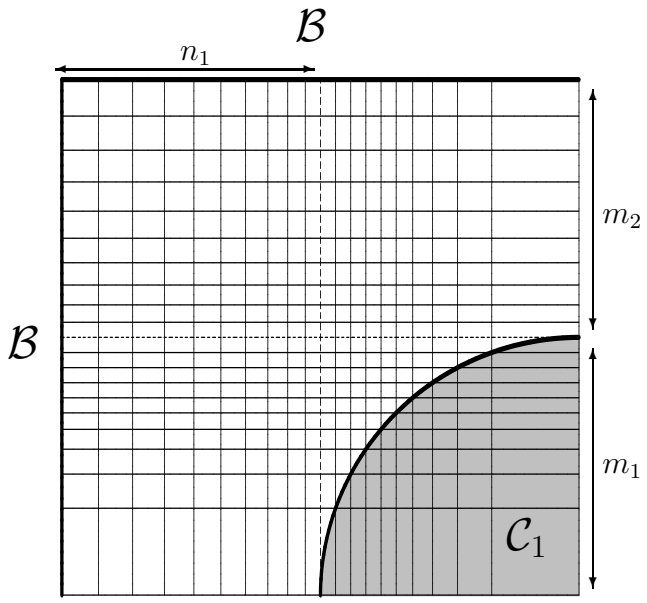

Figure 3:

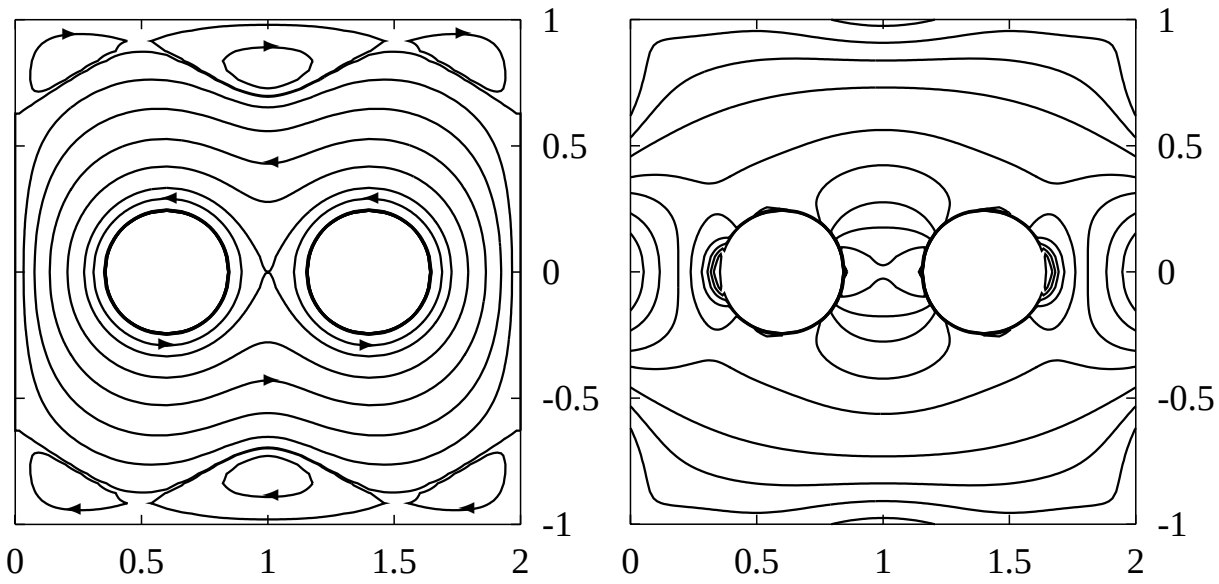

Figure 4:

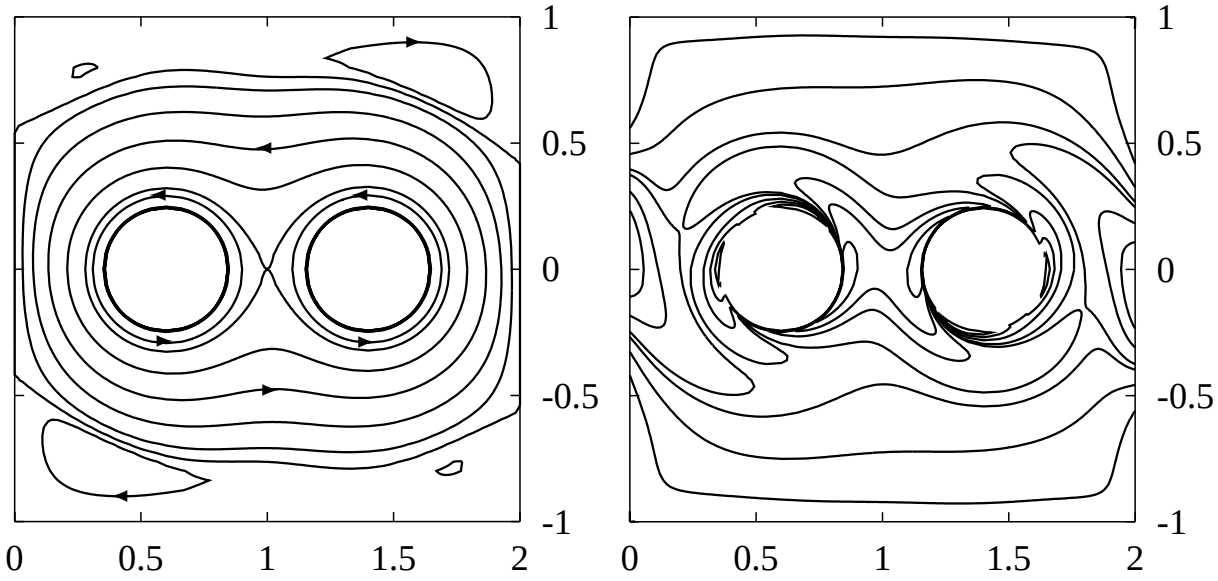

(a)

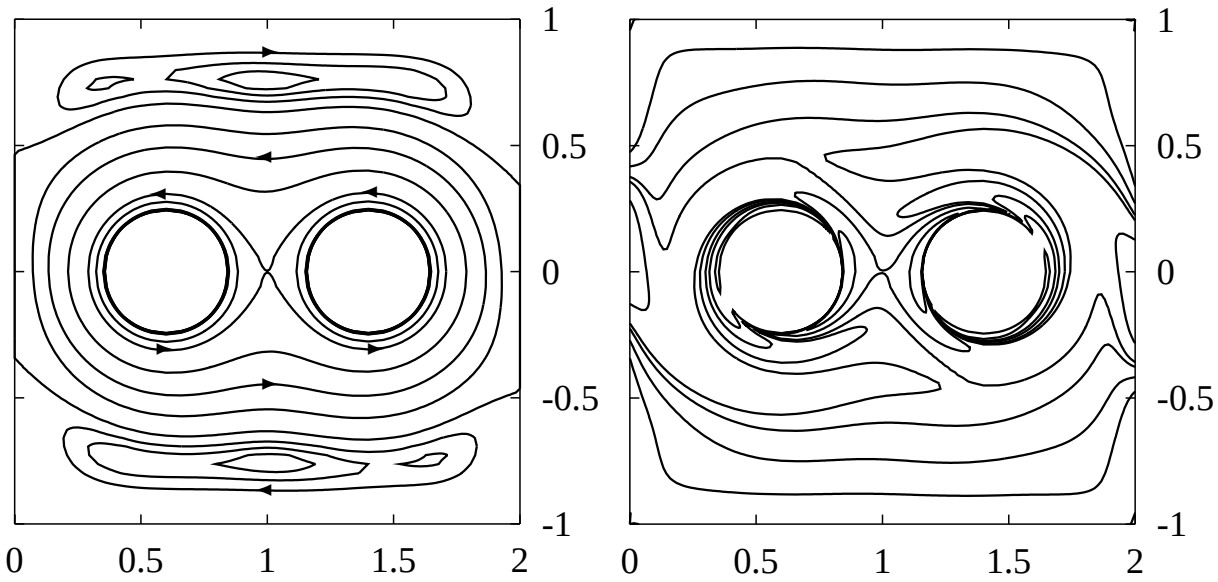

(b)

Figure 5:

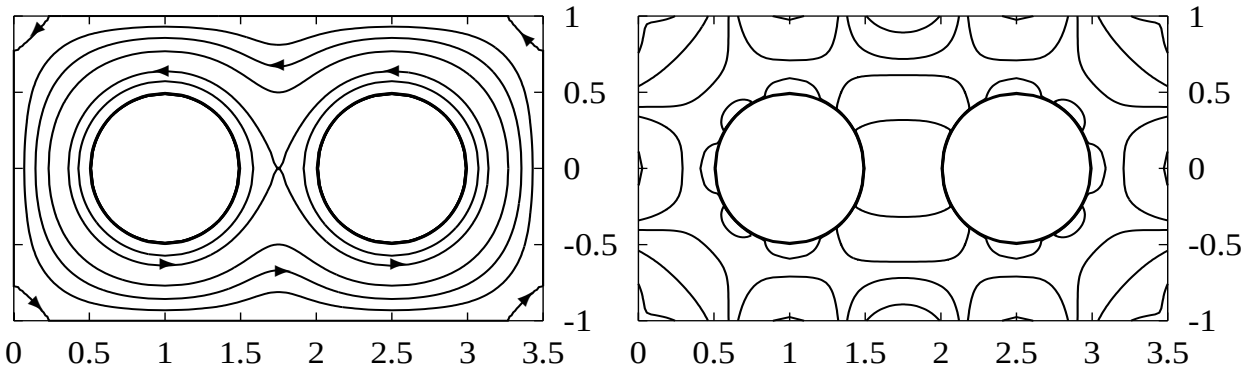
1
0.5
0
-0.5
-1
0 0.5 1 1.5 2 2.5 3 3.5
1
0.5
0
-0.5
-1
0 0.5 1 1.5 2 2.5 3 3.5

(a)

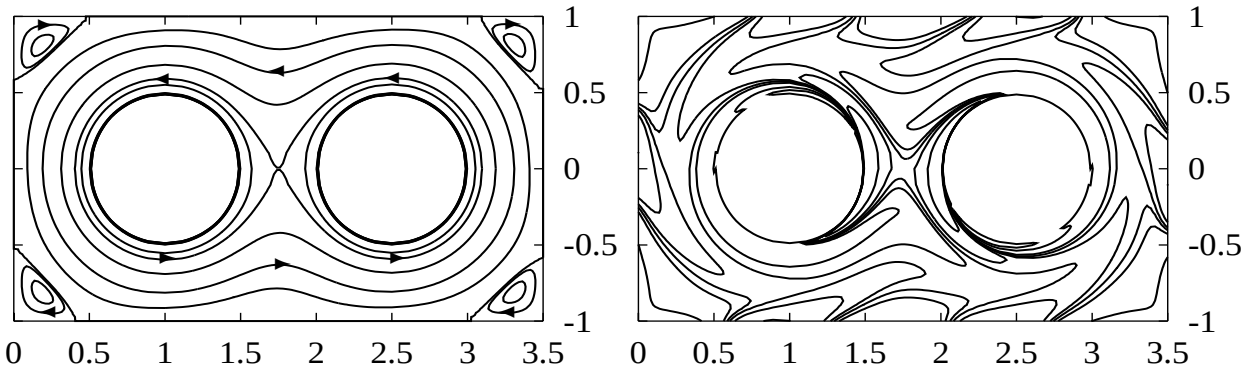
1
0.5
0
-0.5
-1
0 0.5 1 1.5 2 2.5 3 3.5
1
0.5
0
-0.5
-1
0 0.5 1 1.5 2 2.5 3 3.5

(b)

Figure 6:

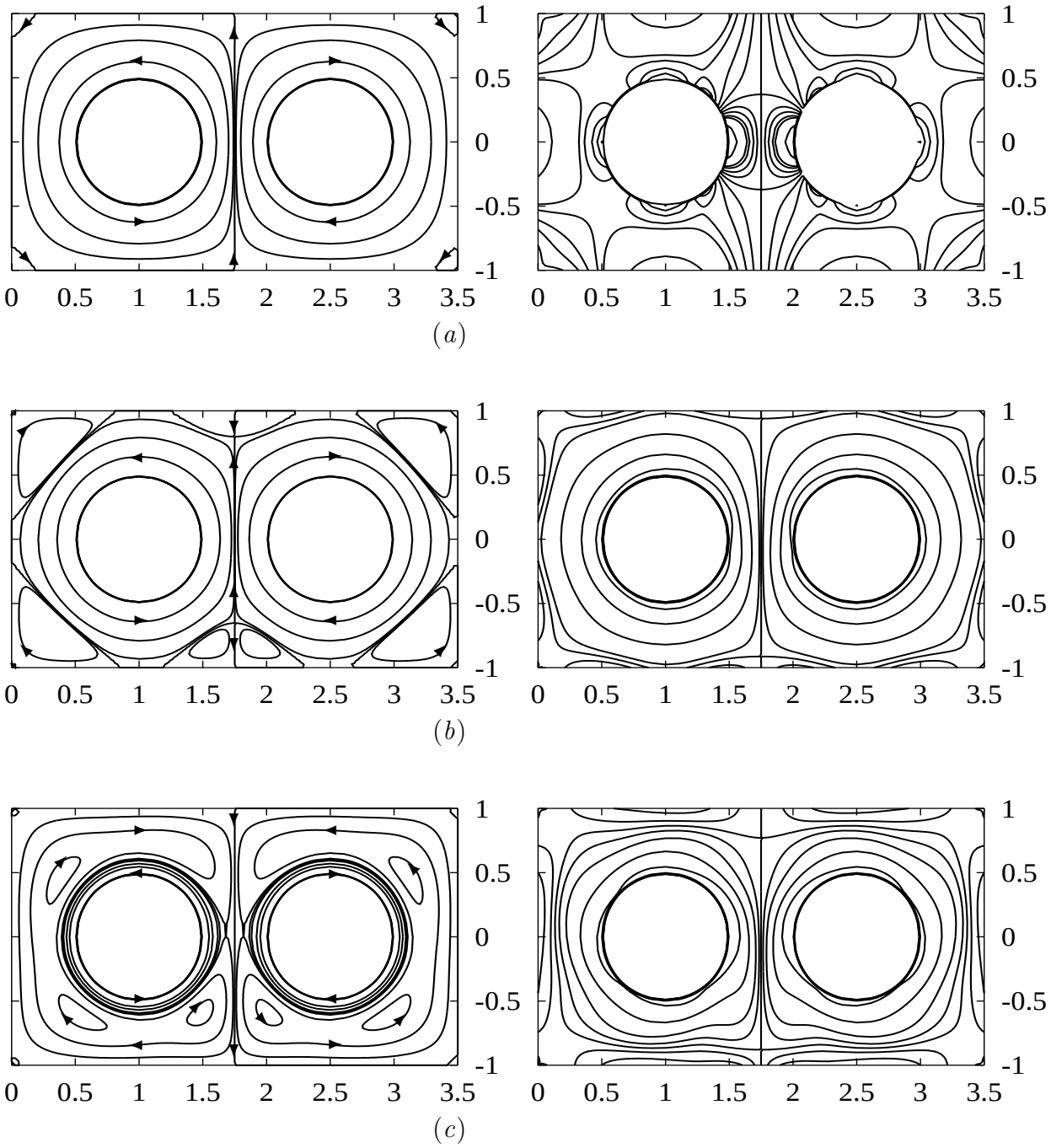

Figure 7:

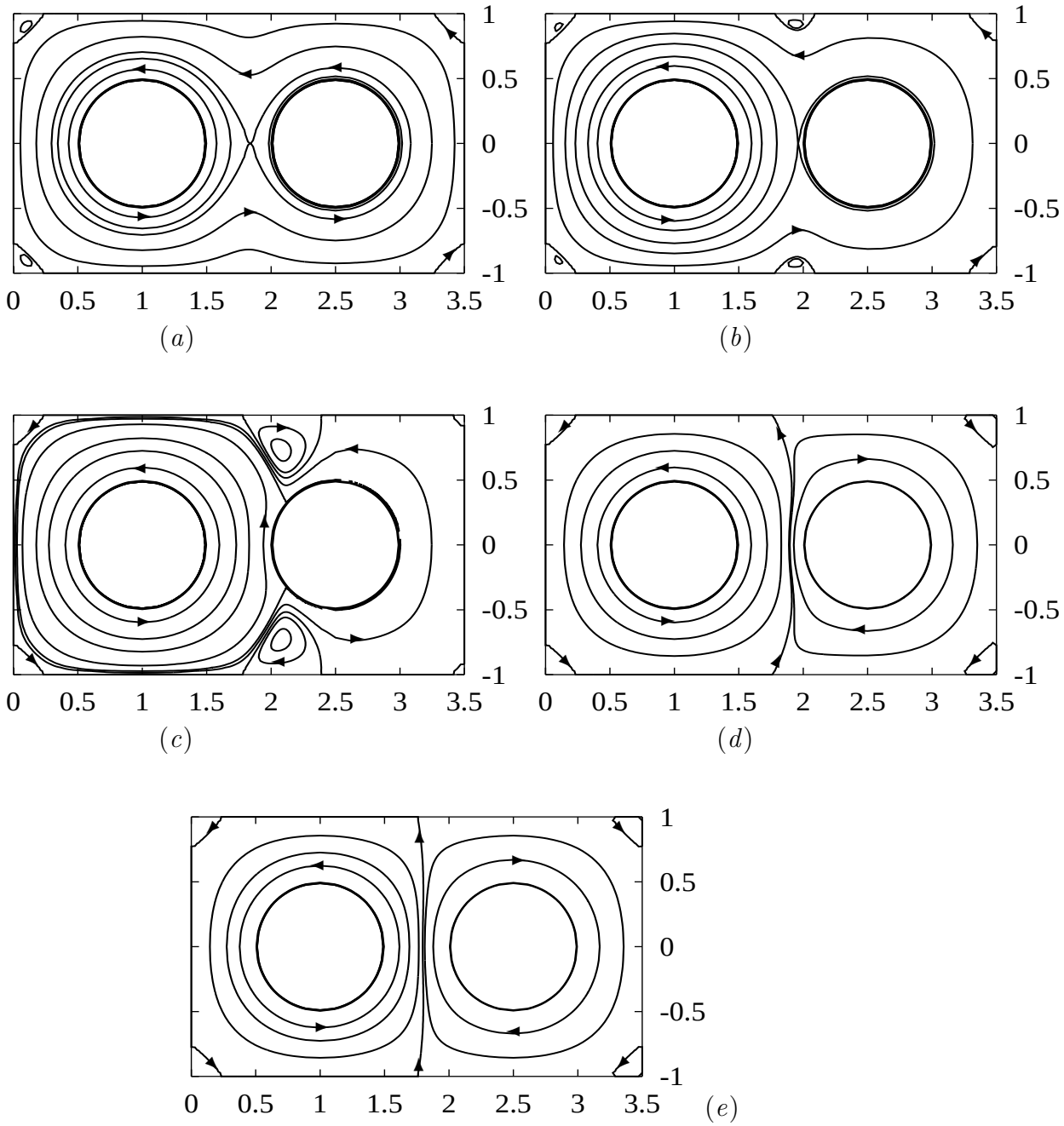

Figure 8:

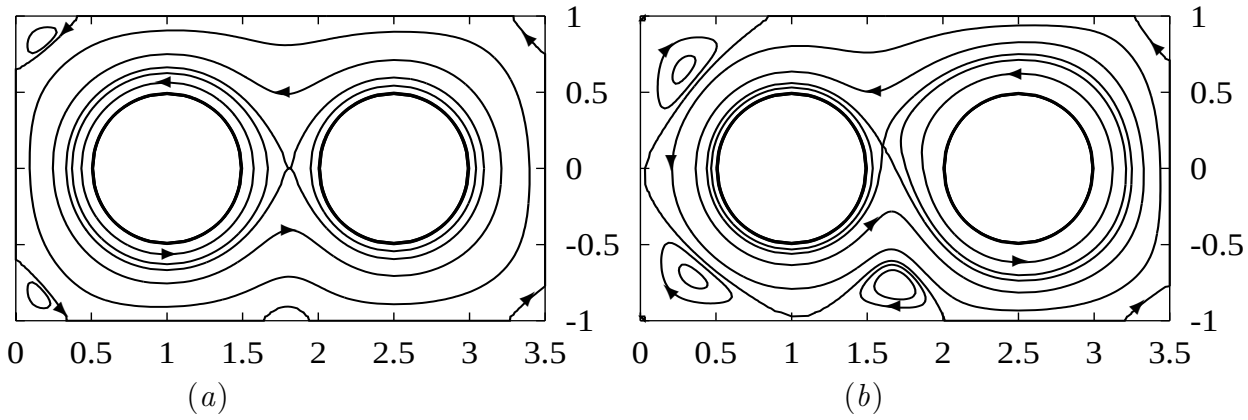

Figure 9:

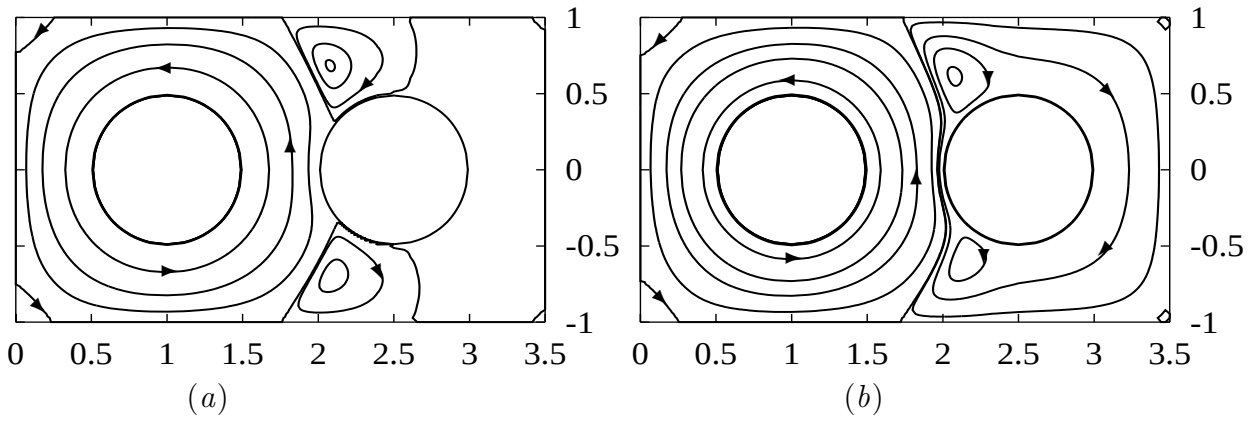

Figure 10:

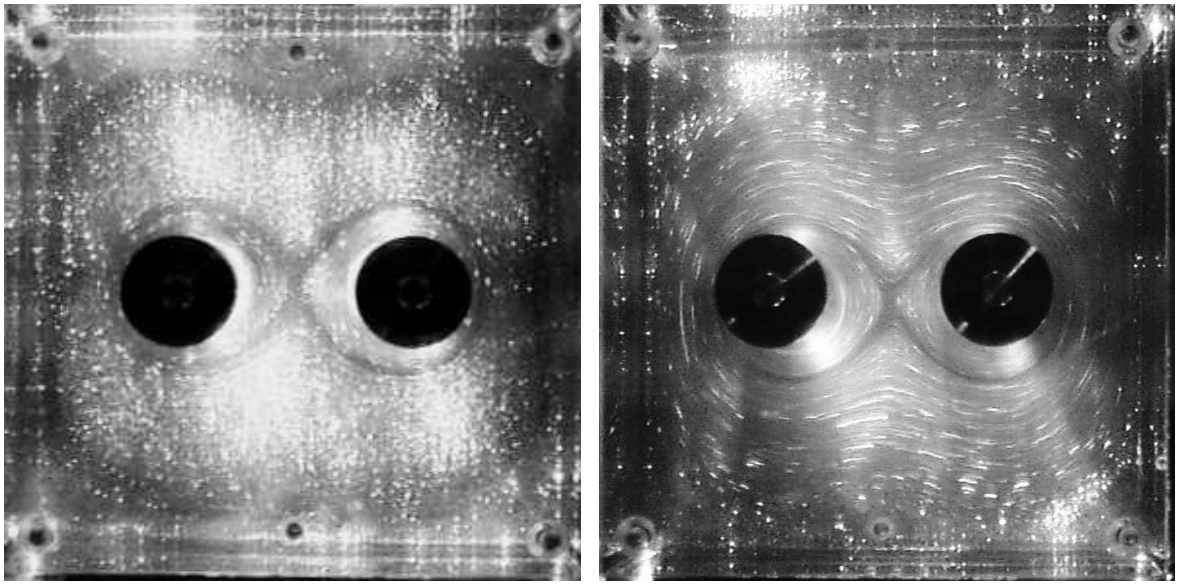

(a) (b)

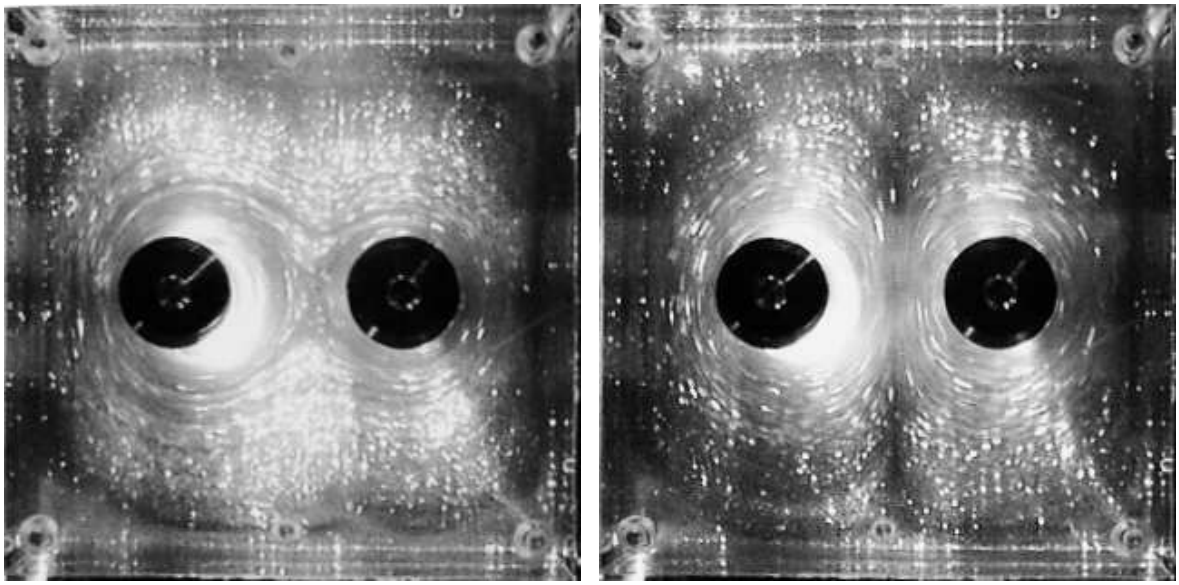

(c) (d)

Figure 11:

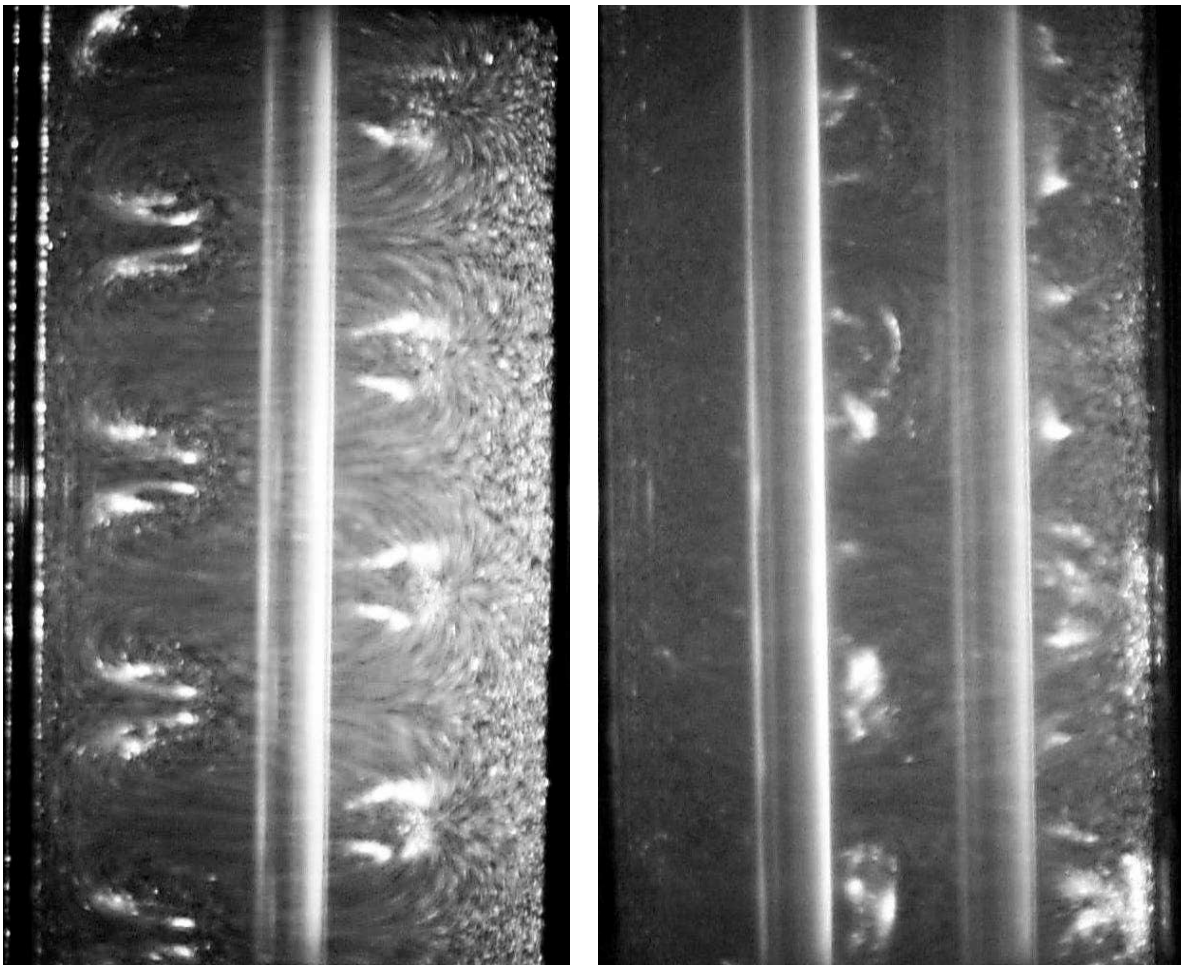

(a) (b)

Figure 12: